PHOTOVOLTAIC POWER FORECASTING USING SKY IMAGES AND SUN MOTION

Arne Berresheim[1] *and Antonio Agudo*[2]

[1]Universitat Pompeu Fabra, Spain
[2]Institut de Robòtica i Informàtica Industrial, CSIC-UPC, Spain

ABSTRACT

Solar energy adoption is moving at a rapid pace. The variability in solar energy production causes grid stability issues and hinders mass adoption. To solve these issues, more accurate photovoltaic power forecasting systems are needed. In intra-hour forecasting, the most challenging issue is high output fluctuations due to cloud motion, which can occlude the sun. Using ground-based sky images, this paper proposes two convolutional neural network models for intra-hour nowcasting and forecasting that incorporate physical information on sun motion and cloud coverage by means of the sun area mean pixel intensity. Particularly, our models exploit that information instead of relying exclusively on photovoltaic output history data as it is standard in state of the art. Taking advantage of sun position and cloud coverage information, we were able to reduce the overall root mean squared error for the nowcasting task, making the model more accurate especially during cloudy days, and obtaining competitive results on forecasting. Moreover, our models are more robust against artifacts such as occlusion and noisy observations.

Index Terms— Photovoltaic Power Estimation, Sun Tracking, Sky Images, Deep Learning.

1. INTRODUCTION

Globally, deployment of solar power and wind is said to be setting new records year by year worldwide until 2030 reaching 40% of the total energy production, while levels in 2021 were at 10% [1, 2]. This staggering increase can be attributed to the global shift towards greener energy in the fight against climate change and geopolitical tensions, such as the Ukraine-Russia conflict. Solar energy has become a more attractive business case, with photovoltaic module costs decreasing by 80% in the last ten years.

Through the rise in photovoltaic (PV) and wind power, the electric grid is forced to adapt with more power system flexibility to maintain electric security [1]. The integration of multiple individual users in micro-grids and large-scale PV farms can lead to imbalances between consumption and generation, resulting in grid stability concerns, which hinder the widespread adoption of solar energy [3]. To address these challenges, accurate prediction of PV power output is crucial for maintaining grid stability and maximizing efficiency, minimizing the need for costly energy storage solutions. Moreover, robust predictions contribute to establishing market equilibrium by enabling effective price determination based on energy resource availability [4].

To achieve reliable predictions the choice of optimal input parameters is vital. Next to the historic PV output information, in [5], meteorological data such as solar irradiance, temperature, cloud coverage, wind speed, air pressure, relative humidity, and perceptible water [4] were exploited. These input data are mostly used for intra-day to day-ahead predictions, ranging from 1 to 48 hours. Persistence models, popular for intra-hour (0-1 hour) forecasting [4], are now primarily employed as baseline models due to their reduction of the problem and limited consideration of weather conditions, such as clouds [3]. It has been demonstrated that techniques like k-Nearest Neighbor, persistence models, and autoregressive integrated moving average are outperformed by artificial neural networks [6], especially in scenarios involving cloudy or partly cloudy days with uncertain meteorological conditions. These situations are more complex tasks, necessitating a greater amount of input data and advanced models.

Solar irradiance denotes the fraction of solar energy emitted by the sun that reaches the Earth's surface. A study in Malaysia [5] has shown that solar irradiance correlates with PV power output with a factor of 0.98. The major factors that determine solar irradiation are the solar zenith angle, the angle between the vertical and the sun, and cloudiness. Therefore in clear sky conditions the solar zenith angle with air mass can model the situation easily as shown in [7]. Some image processing techniques have been proposed to deduce the sun position and solar zenith angle from sky images [8].

Cloudiness is a highly local matter determined by factors such as wind speed and cloud type. Clouds move at different speeds, heights, they overlap and remain non-fixed [9] shapes with splitting, merging and deformation happening constantly. Making cloud recognition, modelling and forecasting such a complex endeavour [10, 11]. From sky images information about cloud position can be extracted by thresholding or adaptive thresholding [12]. A more complex approach is seen in [13], combining block matching, optical

This work has been supported by the project MoHuCo PID2020-120049RB-I00 funded by MCIN/ AEI /10.13039/501100011033.

flow and SURF [14] feature matching algorithms for cloud recognition, classification and motion prediction. For better accuracy in cloud recognition advanced image segmentation techniques have also been employed in [15].

Another class of inputs are 2D images which are commonly employed for more detailed information on cloud recognition, tracking and forecasting [10] as in [3, 16]. Satellite imaging has been employed in [17], but the images do not entail both high temporal and spatial resolution and, therefore, they are impractical [18]. Ground based sky image datasets have been collected to help facilitate the forecasting task [19, 20] and are often applied in intra-hour forecasting tasks using Convolutional Neural Networks (CNNs) [3, 21]. To improve the results, weather condition specific sub-models [20] as well as new ways to merge graphical and numerical data were proposed [22]. Another possibility is to use image pre-processing techniques to extract cloud information in the form of cloud binary maps and velocity fields [3]. Given that most systems feed the model a sequence of images, this means that temporal information is only learned implicitly [10]. Therefore new techniques have been developed such as merging Long-short Term Memory (LSTM) cells with CNNs [23]. Results have shown that incorporating cloud knowledge into image-based forecasting models improves accuracy [10].

Inspired by [3, 7], in this work we propose a PV output nowcasting and forecasting model that exploits physical priors. With domain knowledge and image processing techniques new valuable information will be inferred and considered as additional input to our model. Thanks to our novel neural models, our estimations outperform those provided by competing approaches while the solution is more robust.

2. NOWCAST AND FORECAST NEURAL ARCHITECTURES

We now present our neural architectures for nowcast and forecast PV power estimation. In the first case, our method applies a simple mapping, taking a single image as input and directly predicting the PV output in kilo Watt (kW) related to the image. In the second case, our model takes images of the last 16 minutes, concatenated in the color channel, and PV power production of the last 16 minutes as input. Exploiting that, the algorithm can return a prediction for the PV output in 15 minutes. A summary of both models is displayed in Fig. 1.

As it can be seen, the architecture of the two models are quite similar. They both consist of two blocks with convolutional layers with 3×3 filters with a stride of 1 and same-value padding, having 24 and 48 filters, respectively; as well as batch normalisation. The activation function applied throughout all layers is a rectified linear unit function, useful to provide a non-linear behaviour as it does not return negative values. Finally the last part of the block being a 2×2 pooling layer with a stride of 2. After flattening the tensors the data

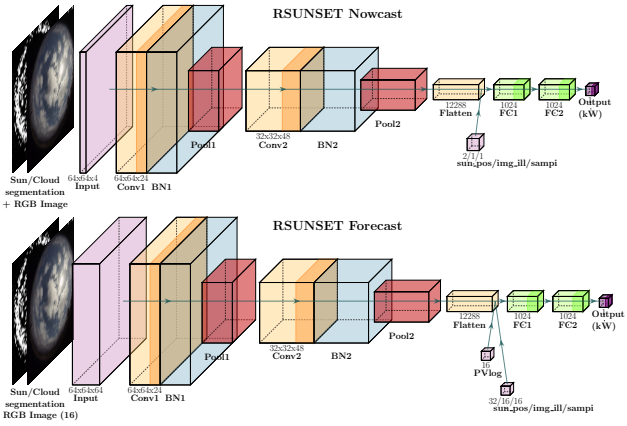

Fig. 1. **Neural architectures for PV power estimation.** Every block includes sequentially a convolutional, a batch normalization and a pooling layer. After that, the processed input is flattened and concatenated with different information. **Top:** Nowcast model. **Bottom:** Forecast model.

are sent to the third and last block, which consists of two Fully Connected (FC) layers with 1,024 neurons each and a dropout of 40% to enhance stability of the model. It is in this part where the main difference between the two models appears, as in the forecast model the historical PV data is concatenated to the flattened tensor before the FC layers.

A powerful methodology to boost performance is developing priors with domain knowledge. An example of prior usage could be to apply a temporal smoothness prior, because the PV outputs continuous shape as a function of a smooth variation in the input image. As described earlier the model's weakness lies in cloudy conditions where high fluctuations in PV output cannot be accurately predicted and PV output is not smooth. Therefore a smooth prior would not increase model performance. To better model these fluctuations, in this paper we consider different loss functions to the model, like Mean Absolute Error (MAE), mean absolute percentage error, mean squared logarithmic error, pseudo Huber loss and Log cosh. In the corresponding loss function we are looking to penalise large errors, while maintaining the accuracy in the sunny days. The fluctuations occur due to clouds occluding the sun. Hence, in our approach we extract information on sun and cloud position from the images and add them as additional input to the model. Unfortunately, our dataset does not contain ground truth information about neither the sun position nor the cloud segmentation, and therefore, we propose an algorithm to obtain them.

We develop five new models. To this end, five additional input variables were extracted from the ground-based sky images (image illumination, cloud segmentation, sun segmentation, sun position and, sun area mean pixel intensity or SAMPI) described in the next paragraphs. To consider that, the information is included in the model's architecture as can be seen in Fig. 1, for both nowcast and forecast models. Particularly, sun or cloud segmentation involves adding a

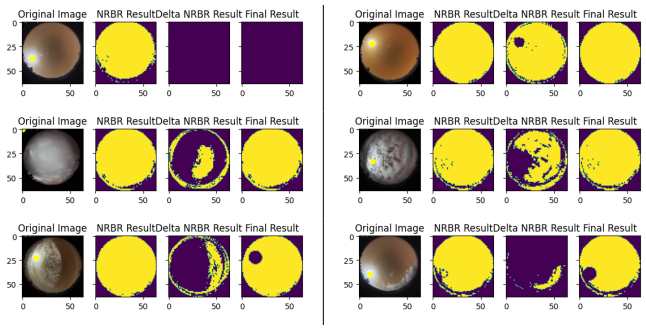

Fig. 2. **Example results of the cloud segmentation algorithm.** The same information is provided twice. The figure displays from left to right: the ground-based sky images, its NRBR threshold result, ΔNRBR result and the final one.

fourth channel to the input image. Moreover, a second variation aims to leverage numerical information, including sun position, total image illumination, and SAMPI. These values are concatenated to the tensors between the convolutional and FC blocks, similar to the historical PV log term in the forecast model. After evaluating their partial contributions, we combine some of them to obtain improved results.

Cloud segmentation. This problem is very challenging in image processing and computer vision. We implement the approach outlined in [12] employing thresholding techniques to classify each pixel into cloud (1) and non-cloud (0) pixels, returning a percentage cloudiness value. It relies on Rayleigh's scattering law from which we can deduce that clear skies spread more blue than red light and cloudy skies spread a similar amount of blue and red light. The metric used is the normalised blue-red-ratio (NRBR) from [24] and the ΔNRBR utilising background subtraction from a sunny day library to counteract the high pixel intensity in the circumsolar area. The approach and the threshold values were developed on the same dataset that is used in this work [20]. Therefore, we use it without any adjustments, but utilising the cloud segmentation instead of the calculated cloudiness value.

Some example results of the cloud segmentation on selected test days are shown in Fig. 2. We can see that the segmentation results are faulty having issues both in clear sky conditions as well as in cloudy ones. Some clear sky images contain a red cast, which impedes the usage of Rayleigh's scattering law and delivers incorrect results. More issues occur when the sun position cannot be determined, as the background subtraction loses its advantage.

Sun Motion Tracking and Sun Area Mean Pixel Intensity. For sun motion tracking with 360-degree camera sky images, we follow the ideas in [8]. Firstly the image is converted into a gray-scale image. Then a threshold $P_{th} = 225$ is applied to determine the area of the sun (*sun segmentation*). High cloud coverage in certain images could cause no pixels to surpass the threshold, resulting in no sun detection. We have experimentally optimized the trade-off between precision and number of false negatives, selecting the provided threshold. After that, the algorithm has to get the center pixel of the sun segmentation, i.e., the *sun position*. When no pixel passes the threshold, the sun segmentation is an image of zeros and the sun position is declared as (0,0).

A metric that combines information about sun position and cloud coverage is SAMPI [12], that can be defined as SAMPI $= \frac{1}{N}\sum_{i\in S} I_i$, where $I_i = 0.229R_i + 0.587G_i + 0.114B_i$ for the i-th pixel with $i = \{1, \ldots, N\}$ being N the number of samples, and S represents the set of pixels with a radius of 7 around the sun. As the cloud coverage in the circumsolar area is especially important, radius needs to be high enough to entail greater information, as sunny and cloudy conditions provide different levels of pixel intensity. Again, when no sun position was deduced we let SAMPI$= 0$.

In both models a MSE$(y, \hat{y}) = \sum_{i=1}^{N}(y_i - \hat{y}_i)^2$ loss is applied as it provided the best performance, where y and $\hat{y}$ denote the ground truth value and the prediction, respectively. For training, an Adam optimizer with a batch size of 256 and 10-fold cross validation is applied to obtain stable results.

3. EXPERIMENTAL EVALUATION

First of all, we present the dataset we use in this paper, that it contains ground-based sky images recorded at 20 Hz at high resolution (2048×2048) with a 360-degree fish-eye camera from 06:00AM to 08:00PM from March 2017 to December 2019, and they are paired with PV history data recorded at a 1-min frequency. As in [20], we use 363,375 samples of sky images with a temporal resolution of one minute and spatial resolution of 64×64, as well as the corresponding PV output. From the previous data, we deduced another dataset ourselves for the forecasting task, also referred to as the Forecast dataset, with half the size (174,816 samples) by applying a two minute sampling rate each day. To make a fair comparison, we consider the same training, validation and testing split as was used in [20], i.e., 96/4, respectively. Due to the fact that our dataset does not contain annotations about the sky conditions of each image we concluded that experiments were not feasible. For quantitative evaluation, we propose the Root Mean Squared Error RMSE$(y, \hat{y}) = \sqrt{\sum_{i=1}^{N}(y_i - \hat{y}_i)^2}$, and the MAE as suggested in [20].

In Table 1 we provide our experimental results for nowcast and forecast PV power tasks for SUNSET [20] model, our own implementation of the SUNSET model denoted as RSUNSET, and this neural model together with different knowledge priors one by one (image illumination, cloud segmentation, sun segmentation, sun position, SAMPI) to finally consider the combination of sun position and SAMPI. SUNSET [20] model provides an overall RMSE test error of 2.43kW and 3.03kW for nowcast and forecast tasks, respectively. It is worth noting that the difference in performance between sunny (0.8/0.61kW) and cloudy (3.34/4.27kW) days

for nowcast/forecast, respectively, being the cloudy scenario more challenging.

Regarding our estimations, the use of image illumination worsened the error slightly, especially during the sunny test days. The segmentation information lowered the models performance significantly up to 2.715 overall RMSE. The sun position and SAMPI give similar results as the baseline, only varying up to 0.035 in the overall RMSE. The SAMPI model performs similarly to the sun position model on sunny days, but the last provides the best results on cloudy days, even outperforming the baseline. On balance, just SAMPI and sun position seem to show promising results and, therefore, we only consider these contributions to be exploited in our final model. To this end, our final model takes both parameters as additional input, concatenated before the FC layers in the nowcast and forecast architectures. We will discard the other parameters, as they did not add any valuable information, at least after considering the segmentation estimation. Image illumination does not correlate with PV output. The underperformance of bitmap segmentation inputs could be linked to the unsuitability of the fourth image channel for model training. Regarding cloud segmentation results, the added information's quality is problematic, as discussed earlier. Our final model outperforms the original one in a nowcast task in all error metrics, improving its overall RMSE by 0.027kW. The hike in performance is especially notable during the cloudy test days with a 0.04kW difference in the RMSE, where it better models the high variance. The combination of sun position and cloud coverage can give us more complete information on the PV output. A qualitative evaluation in ten test days is displayed in Fig. 3.

Unfortunately, we were not able to reproduce the results of the forecast model, because we deduced the dataset ourselves. Although we followed the same steps outlined in the original papers [20, 3] we obtained an overall RMSE 5.67kW higher than the original. In any case, our forecast model can consistently outperform the reproduced model in all the metrics, showing the effectiveness of the physical priors we propose in this paper.

Finally, we evaluate the robustness of our model against occlusions and noisy observations on the test set. For missing data, we synthetically produce an occlusion in the image of size 9×9 pixels. The same coordinates are used for one test day, as this is the most realistic setup. Regarding the noise evaluation, we apply Gaussian noise with a variance equals to 0.1. Pixels outside the value range of 0 to 1 are changed to the corresponding edge value. As expected, both artifacts worsened performance significantly with the 9×9 occlusion and the noisy observations. For nowcast, on the one hand the overall RMSE is 2.96kW and 7.64kW by applying SUNSET [20] model, exceeding the value of 2.43kW obtained under normal conditions (see Table 1). On the other hand, the overall RMSE by applying our proposed model (RSUNSET+sun position+SAMPI) in the same conditions is 2.78kW and 6.98kW, respectively. Comparing the numbers, it can be seen as our model achieves more robust estimations against artifacts than competing approaches.

Model	Overall (kW)		Sunny days (kW)		Cloudy days (kW)	
	RMSE	MAE	RMSE	MAE	RMSE	MAE
SUNSET [20]*	2.43	1.50	0.8	0.66	3.34	2.34
RSUNSET (Ours)	2.44	1.52	0.85	0.70	3.35	2.34
+image illumination	2.47	1.56	0.88	0.73	3.37	2.38
+cloud segmentation	2.71	1.74	1.00	0.75	3.70	2.72
+sun segmentation	2.53	1.61	0.89	0.71	3.46	2.50
+sun position	2.43	1.52	0.84	0.69	**3.33**	2.34
+SAMPI	2.46	1.54	0.83	0.69	3.38	2.38
+sun position & SAMPI	**2.40**	**1.48**	**0.79**	**0.65**	**3.30**	**2.30**
SUNSET [20]*	**3.03**	**1.71**	**0.61**	**0.50**	**4.27**	**2.95**
RSUNSET (Ours)	8.70	7.18	9.22	8.16	8.15	6.20
+sun position & SAMPI	**8.13**	**6.65**	**8.62**	**7.55**	**7.61**	**5.75**

Table 1. **Nowcast and forecast PV power predictions in sunny and cloudy days.** Nowcast (top) and forecast (bottom) results as a function of several priors. * results taken from [20].

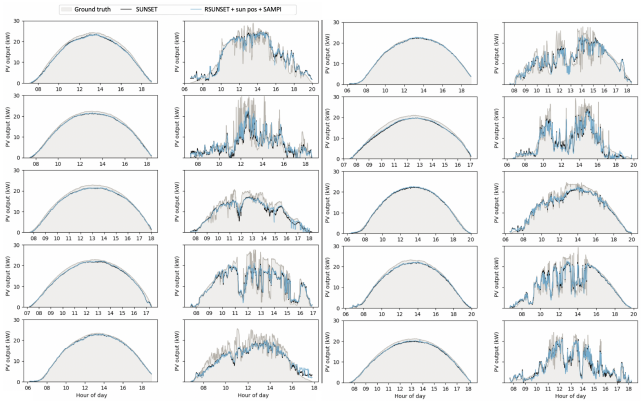

Fig. 3. **Qualitative comparison on nowcast estimation.** The same information is provided on both sides, including ground truth, SUNSET [20] and our RSUNSET+priors. Five test days on sunny (left) and cloudy (right) conditions.

4. CONCLUSION

In this paper we propose several neural models for nowcast and forecast PV power estimation from RGB visual signals. While current approaches solve the problem directly from data, some properties are not correctly learned by the neural network, limiting the performance of the model. In contrast, in this work, ground-based sky images are exploited to infer some physical properties such as the sun position and cloud coverage that are then combined with the input images to learn a more accurate and effective model. Thanks to that, our nowcast and forecast models successfully outperform state-of-the-art approaches, being even more robust than those against occlusion and noise artifacts. We believe our analysis can help improve the new generation of algorithms in this topic, exploiting a data-driven model where physical priors are extracted and incorporated in the main pipeline.

5. REFERENCES

[1] L. Cozzi, T. Gould, S. Bouckart, D. Crow, T. Kim, C. Mcglade, P. Olejarnik, B. Wanner, and D. Wetzel, "World energy outlook 2020," *IEA*, vol. 2050, pp. 1–461, 2020.

[2] R. Pérez-Gonzalo, A. Espersen, and A. Agudo, "Robust wind turbine blade segmentation from RGB images in the wild," in *ICIP*, 2023.

[3] Y. Sun, V. Venugopal, and A.R. Brandt, "Short-term solar power forecast with deep learning: Exploring optimal input and output configuration," *Solar Energy*, vol. 188, pp. 730–741, 2019.

[4] R. Ahmed, V. Sreeram, Y. Mishra, and M.D. Arif, "A review and evaluation of the state-of-the-art in PV solar power forecasting: Techniques and optimization," *RSER*, vol. 124, 2020.

[5] U.K. Das, K.S. Tey, M. Seyedmahmoudian, M.Y. Idna Idris, S. Mekhilef, B. Horan, and A. Stojcevski, "SVR-based model to forecast PV power generation under different weather conditions," *Energies*, vol. 10, no. 7, pp. 876, 2017.

[6] M.Q. Raza, M. Nadarajah, and C. Ekanayake, "On recent advances in PV output power forecast," *Solar Energy*, vol. 136, pp. 125–144, 2016.

[7] Y. Sun, G. Szűcs, and A.R. Brandt, "Solar PV output prediction from video streams using convolutional neural networks," *EES*, vol. 11, pp. 1811–1818, 2018.

[8] G. Garcia-Gil and J.M. Ramirez, "Fish-eye camera and image processing for commanding a solar tracker," *Heliyon*, vol. 5, no. 3, pp. e01398, 2019.

[9] M.K. Yau and R.R. Rogers, *A short course in cloud physics*, 1996.

[10] F. Lin, Y. Zhang, and J. Wang, "Recent advances in intra-hour solar forecasting: A review of ground-based sky image methods," *IJF*, vol. 39, no. 1, pp. 244–265, 2023.

[11] K. Mohammadi and N. Goudarzi, "Study of intercorrelations of solar radiation, wind speed and precipitation under the influence of el niño southern oscillation (enso) in california," *RE*, vol. 120, pp. 190–200, 2018.

[12] Y. Nie, Y. Sun, Y. Chen, R. Orsini, and A. Brandt, "PV power output prediction from sky images using convolutional neural network: The comparison of sky-condition-specific sub-models and an end-to-end model," *JRSE*, vol. 12, no. 4, pp. 046101, 2020.

[13] Z. Zhen, S. Pang, F. Wang, K. Li, Z. Li, H. Ren, M. Shafie-khah, and J.P.S. Catalão, "Pattern classification and PSO optimal weights based sky images cloud motion speed calculation method for solar PV power forecasting," *TIA*, vol. 55, no. 4, pp. 3331–3342, 2019.

[14] H. Bay, T. Tuytelaars, and L. Van Gool, "SURF: speeded up robust features," in *ECCV*, 2006, pp. 404–417.

[15] C. Shi, Y. Wang, C. Wang, and B. Xiao, "Ground-based cloud detection using graph model built upon superpixels," *GRSE*, vol. 14, no. 5, pp. 719–723, 2017.

[16] X. Zhang, Z. Zhen, Y. Sun, F. Wang, Y. Zhang, H. Ren, H. Ma, and W. Zhang, "Prediction interval estimation and deterministic forecasting model using ground-based sky image," *IEEE Trans. Ind. Appl.*, vol. 59, no. 2, pp. 2210–2224, 2023.

[17] S. Rosiek, J. Alonso-Montesinos, and F.J. Batlles, "Online 3-h forecasting of the power output from a BIPV system using satellite observations and ANN," *IJEPES*, vol. 99, pp. 261–272, 2018.

[18] Z. Peng, D. Yu, D. Huang, J. Heiser, and P. Kalb, "A hybrid approach to estimate the complex motions of clouds in sky images," *Solar Energy*, vol. 138, pp. 10–25, 2016.

[19] C. Feng, D. Yang, B.M. Hodge, and J. Zhang, "Opensolar: Promoting the openness and accessibility of diverse public solar datasets," *Solar Energy*, vol. 188, pp. 1369–1379, 2019.

[20] Y. Nie, X. Li, A. Scott, Y. Sun, V. Venugopal, and A. Brandt, "SKIPP'D: a sky images and photovoltaic power generation dataset for short-term solar forecasting," *Solar Energy*, vol. 255, pp. 171–179, 2023.

[21] X. Zhang, Z. Zhen, Y. Sun, Y. Zhang, H. Ren, H. Ma, J. Yang, and F. Wang, "Solar irradiance prediction interval estimation and deterministic forecasting model using ground-based sky image," in *ICPS*, 2022, pp. 1–8.

[22] V. Venugopal, Y. Sun, and A. Brandt, "Short-term solar PV forecasting using computer vision: The search for optimal CNN architectures for incorporating sky images and PV generation history," *JRSE*, vol. 11, pp. 066102, 11 2019.

[23] T.A. Siddiqui, S. Bharadwaj, and S. Kalyanaraman, "A deep learning approach to solar-irradiance forecasting in sky-videos," in *WACV*, 2019, pp. 2166–2174.

[24] Q. Li, W. Lu, and J. Yang, "A hybrid thresholding algorithm for cloud detection on ground-based color images," *JTECH*, vol. 28, no. 10, pp. 1286–1296, 2011.